Conformal Cylindrical Array Sound Source Localization at the Presence of Shadowed Elements

Jiaheng Li, Feng Tong, *Member, IEEE*, Yuehai Zhou, *Member, IEEE*, Yi Yang, and Zhiqiang Hu

Abstract—Sound source localization provides an absorbing capability for unmanned aerial vehicles (UAVs) in scenarios such as search and rescue operations. The shape fusion between the sound array and UAVs forms a special conformal property that is drawing more and more attention. However, the inevitable shadow effect caused by shape fusion seriously degrades the degrees of freedom (DOF) of the array. In this paper, a signal reconstruction-based direction of arrival (DOA) estimation method is proposed to address this limitation. Firstly, we establish a restricted signal model for the conformal cylindrical array (CCA), and then based on frequency domain energy detection, the elements are divided into receiving restricted elements and receiving normal elements. Secondly, according to the position vector of receiving restricted elements, the approximate range of the DOA is roughly estimated to reduce the complexity. Meanwhile, the signals of receiving restricted elements are reconstructed on the basis of receiving normal elements to eliminate the shadow effect and increase the DOF. Lastly, in the estimated approximate range of the DOA, the precise DOA is estimated by peak search. We also derive the 2-D Cramer-Rao lower bound (CRLB) for the CCA. Simulations show that the proposed SR-MUSIC-RS method can achieve satisfactory performance with lower complexity, and the RMSE is close to that of general signal model with normal elements.

Index Terms—DOA estimation, shadow effect, signal reconstruction, CRLB

I. INTRODUCTION

SOURCE localization is essential in Internet of Things (IoT) and has become a research hotspot such as battlefield surveillance, border patrol, search and rescue [1], [2]. In scenarios such as search and rescue operations, unmanned aerial vehicles (UAVs) play a crucial role [3]. While some common visual cues such as image processing or thermal sensing are effective options, the cost associated with such systems is relatively high. As opposed to the conventional visual senses, acoustic source localization which relies on auditory senses is an important function for UAVs and becomes an emerging area in search and rescue operations [4], [5].

Direction of arrival (DOA) estimation is one of the core researches in the field of array signal processing and can be used to resolve the acoustic source localization problem. Many classic DOA estimation algorithms including multiple signal classification (MUSIC), Capon, and their variants, have been wildly developed for different accuracies and complexities [6]. Deep learning-based methods, provide a potential way to locate the source by data-driven, e.g., convolutional neural network (CNN), generalized regression neural network (GRNN), etc. [7], [8] However, those methods need to learn the hidden mapping relationship between the received signals and DOAs, which requires a large amount of training data and suffers from environment sensitivity. [9] In addition, most of the above algorithms are based on conventional array formation such as linear or planar array and thus unable to meet the booming requirement of UAVs from the perspective of streamline shaping, aerodynamic drag reduction, space-saving, etc. [10]

Unlike the above conventional array that exhibits an explicit array formation, conformal array is a type of flexible array that does not change the shape of carrying vehicle, such as spherical conformal array, conical conformal array, cylindrical conformal arrays (CCA), and other irregular conformal arrays [11]. Therefore, UAVs equipped with conformal array for DOA estimation have many benefits including wide-angle coverage, reduction of cross-section, easy installation, etc. [12]

Recently, the research on DOA estimation using conformal array has gained great concern [13], [14]. Sharifi *et al.* [15] designed a hemispherical antenna structure with 3 different tilts and 13 directive circular patch antennas to overcome the tilt effect and proposed a tilt optimization method to increase the DOA estimation accuracy. Mohammadi *et al.* [16] derived the 2-D Cramer-Rao lower bound (CRLB) of a truncated hexagonal pyramid conformal array with 7 patches and proved that conformal array can achieve better DOA estimation performance than that of planar array, especially at the horizon angles. To improve the estimation performance with low SNR and small snapshots, Lan *et al.* [17] proposed a novel 2-D DOA estimation approach based on tensor technique, the multidimensional information, and cross-covariance tensor method are utilized to estimate a more precise DOA. To decrease the computational complexity, Wu *et al.* [18] proposed a novel algorithm by combining geometric algebra with MUSIC to estimate DOA for CCA.

However, in contrast to traditional arrays, conformal array exists the "shadow effect" because of the curved shape of carrying vehicle, especially for CCA, which means that some elements of the array may be blocked by the curved shape, i.e. cannot receive the signal from the source, resulting in the significant degradation of DOA estimation precision [19]. To

Jiaheng Li, Feng Tong and Yuehai Zhou are with the College of Ocean and Earth Sciences, and the National and Local Joint Engineering Research Center for Navigation and Location Service Technology, Xiamen University, Xiamen 361001, China. (e-mail: lijiaheng1009@163.com; ftong@xmu.edu.cn; zhouyuehai@xmu.edu.cn).

Yi Yang and Zhiqiang Hu are with the Shenyang Institute of Automation, Chinese Academy of Sciences, Shenyang 110169, China. (e-mail: yangyi@sia.cn; hzq@sia.cn).

cope with this problem, the conformal array is usually divided into multiple sub-arrays with the exact same structure. Liu *et al.* [20] divided the whole array and airspace into several parts and set the assistant sources to reconstruct the manifold of sub-arrays for the direction-finding. Gao *et al.* [21] divided the CCA into several subarrays to obtain the complete output vector and used the cross-correlation matrix of the subarrays to eliminate the noise vector. By dividing a cylindrical conformal array into 8 subarrays, Yang *et al.* [22] proposed a sub-array-based MUSIC algorithm (S-MUSIC) for DOA estimation. Further, combined with the sub-array divided technique and interpolation technique, Yang *et al.* [23] proposed a novel DOA finding method for conformal array applications. Based on rotational invariance techniques, this method can accurately and quickly estimate the 1-D and 2-D directions of arrivals. Alinezhad *et al.* [24] employed the nested array principles to solve the underdetermined DOA estimation. The shadow effect is eliminated by transforming each selected sub-array to virtual nested arrays, meanwhile, the interpolation error is reduced, and the MUSIC is finally applied for DOA estimation. To avoid measuring the shadowing effect, Yang *et al.* [25] separated the azimuthal angle from all the unknown information and estimated the azimuthal angle by the rank reduction (RARE) algorithm.

Although the above-mentioned sub-array divided type methods are capable of overcoming the shadow effect by only utilizing the elements that received the incident signal, ignoring those elements affected by the shadow effect will inevitably lead to loss of the degrees of freedom (DOF) of the array, as well as the performance degradation of DOA estimation.

In this paper, we proposed a signal reconstruction-based DOA estimation method instead to mitigate the shadow effect. Specifically, the restricted signal model is firstly established to analyze the relationship of different types of elements. Then, based on frequency domain energy detection, the elements are divided into receiving restricted elements and receiving normal elements. And the approximate range of the DOA can be roughly estimated according to the position vector. Meanwhile, the signals of receiving restricted elements are reconstructed based on that of receiving normal elements. Lastly, in the estimated approximate range, the precise DOA is estimated by peak search. We also derive the 2-D CRLB for the CCA. Simulations validate that the proposed method can achieve more satisfactory performance than the traditional methods.

The rest of this paper is organized as follows. Section II introduces the general signal model and restricted signal model, respectively. Section III presents the proposed signal reconstruction-based DOA estimation method. The CRLB is derived in Section IV. In Section V, the effectiveness of the proposed method is verified by simulations. Finally, Section VII concludes the paper.

II. SYSTEM MODEL

Without loss of generality, a simplified scenario of a CCA onboard a cylindrical carrier is considered as given in Fig. 2(a), where S is the tag of the source in the three-dimensional space at the Cartesian coordinate system, and S' is the projection
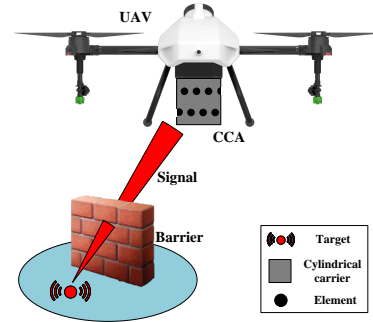
Fig. 1. Sound source localization in search and rescue operations via UAV.

(a) 3-D view   (b) Top view
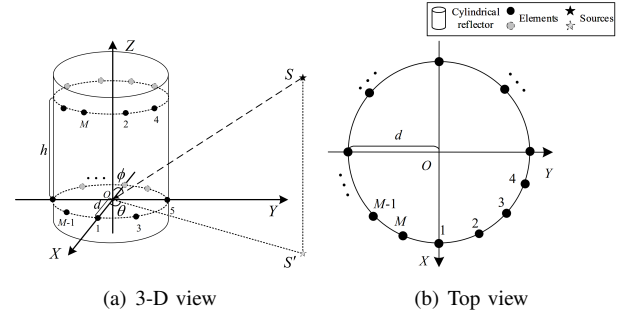
Fig. 2. Conformal array receiving model with a cylindrical carrier.

of source S on the X-Y axis. The number of array elements distributed on the surface of a cylindrical carrier is $M \geq 6$, and is divided into two layers shown in Fig. 2(a). The upper and lower layers are alternately distributed. Thus, viewed from the Z-axis, elements are presented as a uniform circular array shown in Fig. 2(b). The radius of the cylindrical carrier is d, and the distance between the two elements in the Z-axis of the cylindrical carrier is h, which define the size of the array together. Each element is defined by the position vector $\mathbf{r}_m = [\mathrm{x}_m, \mathrm{y}_m, \mathrm{z}_m], m = 1, ..., M$.

The incident signal from a single far-field narrowband source located at an arbitrary direction vector (θ, ϕ) generates waves, where $\theta \in [0°, 360°)$ is the azimuth angle and $\phi \in [0°, 180°)$ is the elevation angle. Then, the propagation vector $\boldsymbol{v}(\theta, \phi)$ can be expressed as

$$\boldsymbol{v}(\theta, \phi) = [\cos(\theta)\sin(\phi), \sin(\theta)\sin(\phi), \cos(\phi)]^T, \quad (1)$$

where $(\cdot)^T$ denotes the transpose.

A. General signal model

Ignoring shadow effect, all the elements, which are regarded as receiving normal elements, can receive the incident signal directly. The steering vector $\boldsymbol{\alpha}(\theta, \phi) \in \mathbb{C}^{M \times 1}$ can be written as

$$\boldsymbol{\alpha}(\theta, \phi) = [\alpha_1(\theta, \phi), \alpha_2(\theta, \phi), \cdots, \alpha_M(\theta, \phi)]^T, \quad (2)$$

where $\alpha_m(\theta, \phi) = e^{(-j\omega \mathbf{r}_m \boldsymbol{v}(\theta, \phi))}$ is the response between the m-th element and source. $\omega = 2\pi/\lambda$, and λ is the wavelength of the signal. Then, the array output $\boldsymbol{x}(n) = [x_1(n), x_2(n), ..., x_M(n)]^T \in \mathbb{C}^{M \times 1}$ at the time instant n can be expressed as

$$\boldsymbol{x}(n) = \boldsymbol{\alpha}(\theta, \phi)s(n) + \boldsymbol{e}(n), \quad (3)$$

where $s(n)$ is the source signal which is considered as sinusoidal signal with defined frequency and amplitude, $\boldsymbol{e}(n) = [e_1(n), e_2(n), ..., e_M(n)]^T \in \mathbb{C}^{M \times 1}$ is the additive noise with zero mean value and uncorrelated with the source $s(n)$. The probability density function (PDF) of $\boldsymbol{e}(n)$ is $N\left(0, \sigma_e^2\right)$, and σ_e^2 is the noise variance. Moreover, the motion of UAV and wind will bring inevitable relative motion of the array, which is called "Doppler spread" and will cause the frequency shift of the received signal. Considering that the CCA carried on UAV can remain relatively static while the UAV is hovering, and the flourishing doppler estimation and compensation algorithms, the "Doppler spread" is not regarded as the core issue in this paper. Thus, the main objective of this paper is to estimate the DOA of source according to Eq. (3).

The classic MUSIC (C-MUSIC) algorithm estimates the DOAs by peak search in noise subspace. The covariance matrix $R_x \in \mathbb{C}^{M \times M}$ of $\boldsymbol{x}(n)$ is

$$R_x = E\left\{\boldsymbol{x}(n)\boldsymbol{x}^H(n)\right\}, \tag{4}$$

where $(\textbf{.})^H$ denotes the conjugate transpose. Furtherly, R_x can be written as

$$\begin{aligned} R_x &= \boldsymbol{\alpha}(\theta, \phi)E\left\{s(n)s^H(n)\right\}\boldsymbol{\alpha}^H(\theta, \phi) + E\left\{\boldsymbol{e}(n)\boldsymbol{e}^H(n)\right\} \\ &= \delta_s^2\boldsymbol{\alpha}(\theta, \phi)\boldsymbol{\alpha}^H(\theta, \phi) + \delta_e^2\mathbf{I}, \end{aligned} \tag{5}$$

where $\delta_s^2 = E\left\{s(n)s^H(n)\right\}$ is the variance of the source, and $\delta_e^2 = E\left\{\boldsymbol{e}(n)\boldsymbol{e}^H(n)\right\}$. $\mathbf{I}$ is an unit diagonal matrix. The eigendecomposition of R_x can be obtained as

$$R_x = U_s \Sigma_s U_s^H + U_e \Sigma_e U_e^H, \tag{6}$$

where U_s is the signal subspace eigenmatrix corresponding to the large eigenvalue, and U_e is the noise subspace eigenmatrix corresponding to the small eigenvalue. Then, the DOA estimated formula of C-MUSIC under general signal model can be expressed as

$$P_{\text{C}-\text{MUSIC}-\text{GS}} = \frac{1}{\boldsymbol{\alpha}^H(\theta, \phi)U_e U_e^H \boldsymbol{\alpha}(\theta, \phi)}. \tag{7}$$

In practice, the covariance matrix R_x is replaced by

$$\hat{R}_x = \frac{1}{N}\sum_{n=1}^{N}\boldsymbol{x}(n)\boldsymbol{x}^H(n), \tag{8}$$

where N is the number of samples.

B. Restricted signal model

However, due to the occlusion of the existing cylindrical carrier, some elements, which are regarded as receiving restricted elements, cannot receive the incident signal, called the shadow effect. As shown in Fig. 3(a) and Fig. 3(b), since the elements are distributed on the surface of the cylindrical carrier, the elements can only receive the incident signals in the azimuth tangent to the surface, and cannot receive the incident signals in other ranges, resaulting in a reduction DOF.

Without loss of generality, the sources located in the axial inner direction of the cylindrical carrier are ignored. Thus, according to the geometric relationship, for the m-th element,

(a) Front view (b) Top view
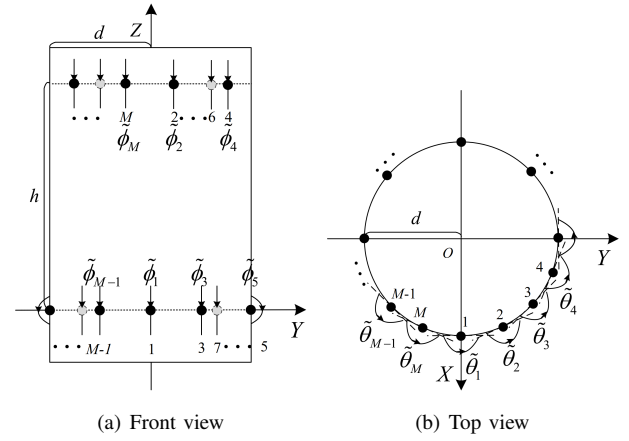
Fig. 3. Schematic diagram of the direction of the received signal for each element.

the range of the azimuth and elevation angles $\left(\tilde{\theta}_m, \tilde{\phi}_m\right)$ over which the incident signal can be received can be denoted as

$$\begin{cases} \tilde{\theta}_m = \left[-\frac{\pi}{2} + \frac{2\pi(m-1)}{M}, \frac{\pi}{2} + \frac{2\pi(m-1)}{M}\right), \\ \tilde{\phi}_m = [0, \pi). \end{cases} \tag{9}$$

That is, the m-th element can only receive the incident signal if the direction vector (θ, ϕ) is within the range of $\left(\tilde{\theta}_m, \tilde{\phi}_m\right)$.

For the array with receiving restricted elements, redefine the occlusion response of cylindrical carrier as $\boldsymbol{O}(\theta, \phi) = \text{diag}\left\{O_1(\theta, \phi), O_2(\theta, \phi), ..., O_M(\theta, \phi)\right\}$, where

$$O_m(\theta, \phi) = \begin{cases} 0, \theta \notin \tilde{\theta}_m \text{ or } \phi \notin \tilde{\phi}_m, \\ 1, \theta \in \tilde{\theta}_m \text{and} \phi \in \tilde{\phi}_m. \end{cases} \tag{10}$$

Therefore, Eq. (3) can be rewritten as

$$\begin{aligned} \boldsymbol{x}(n) &= \boldsymbol{O}(\theta, \phi)\boldsymbol{\alpha}(\theta, \phi)s(n) + \boldsymbol{e}(n) \\ &= \boldsymbol{A}(\theta, \phi)s(n) + \boldsymbol{e}(n), \end{aligned} \tag{11}$$

where $\boldsymbol{A}(\theta, \phi) = [O_1(\theta, \phi)\alpha_1(\theta, \phi), \cdots, O_M(\theta, \phi)\alpha_M(\theta, \phi)]^T$ is the array response. Then, Eq. (4) can be written as

$$\begin{aligned} R_x &= E\left\{\boldsymbol{x}(n)\boldsymbol{x}^H(n)\right\} \\ &= \delta_s^2\boldsymbol{A}(\theta, \phi)\boldsymbol{A}^H(\theta, \phi) + \delta_e^2\mathbf{I}. \end{aligned} \tag{12}$$

Assuming that the k-th element is the receiving restricted element, then, $O_k(\theta, \phi)\alpha_k(\theta, \phi) = 0$. This means that the received signal received by this element only contains noise with a random character of the amplitude and phase. And, the elements at k-th row and k-th column except $R_x(k, k)$ in R_x are all 0, and $R_x(k, k) = \delta_e^2$. In particular, when the phase of the incident signal is disordered, the above-mentioned MUSIC algorithm cannot accurately estimate the DOA based on the receiving restricted elements, leading to significant performance degradation.

III. DOA ESTIMATION METHOD BASED ON SIGNAL RECONSTRUCTION

To eliminate the negative influence of shadow effect on DOA estimation, processing flowchart of the proposed SR-MUSIC-RS algorithm is shown in Fig. 4, which consists of the following steps.
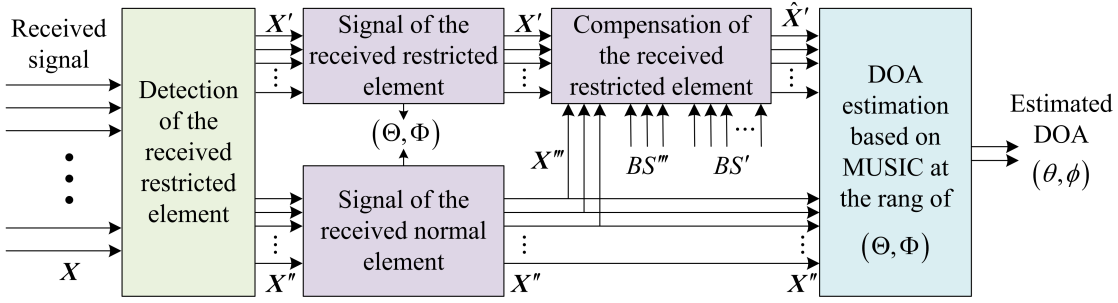
Fig. 4. Process of the processed SR-MUSIC-RS algorithm.

A. Detection of receiving restricted elements

According to the geometric relationship in Fig. 3, the number of receiving restricted elements is at most $\text{ceil}\left(\frac{M}{2}\right)$, where $\text{ceil}(.)$ denotes rounding up, and the serial numbers of the receiving restricted elements are sequential. Since the signal and noise contain different frequency characteristics, this paper converts the received signal to the frequency domain and detects the receiving restricted elements based on frequency domain energy detection.

Suppose that the array out is $x(n) = [x_1(n), x_2(n), ..., x_M(n)]^T, n = 1, ..., N$, then, the frequency-domain received signal can be written as $Y(f) = [y_1(f), y_2(f), ..., y_M(f)], f = 1, ..., F$, where F is the number of fast Fourier transform (FFT) and $y_m = [y_m(1), y_m(2), ..., y_m(F)]$. Define the frequency domain energy of the array is $F_e = [F_e(1), F_e(2), ..., F_e(M)]^T$, where $F_e(m) = \max(|y_m|)$. The proposed detection method of the receiving restricted elements is shown as follows

$$LA(m) = \begin{cases} 1, & F_e(m)/\max F_e > \eta, \\ 0, & F_e(m)/\max F_e \leq \eta, \end{cases} \quad (13)$$

where η is the threshold of frequency domain energy and is set to be $\eta = 0.5$ in this paper. Then, the serial number of zero element in $\{LA(m)\}_{m=1}^M$ represents the receiving restricted elements, where the serial number of one element in $\{LA(m)\}_{m=1}^M$ represents the receiving normal elements.

In addition, after detecting the receiving restricted elements receiving normal elements, the approximate range (Θ, Φ) of the source DOA can be roughly estimated according to Eq. (9), which would greatly reduce the complexity of the algorithm for peak search.

B. Signal reconstruction of receiving restricted elements

The signal reconstruction of receiving restricted elements is based on the signals received by normal elements. For simplicity, the total number of array elements is considered as $M = 8$ in this case, then, the position vector of each element is $\{[x_m, y_m, z_m]\}_{m=1}^8$. Suppose that the receiving restricted elements are $m = 5, 6, 7, 8$, thus, the receiving normal elements are $m = 1, 2, 3, 4$. Then, the occlusion response of cylindrical

carrier is $O_m(\theta, \phi) = 0, m = 5, 6, ..., 8$. And the array output matrix $X = [x_1, x_2, ..., x_M]^T \in \mathbb{C}^{8 \times N}$ can be written as

$$X = A(\theta, \phi)s + E$$

$$= \begin{bmatrix} \alpha_1(\theta,\phi)s + e_1 \\ \alpha_2(\theta,\phi)s + e_2 \\ \alpha_3(\theta,\phi)s + e_3 \\ \alpha_4(\theta,\phi)s + e_4 \\ e_5 \\ e_6 \\ e_7 \\ e_8 \end{bmatrix} = \begin{bmatrix} e^{-j\omega r_1 v}s + e_1 \\ e^{-j\omega r_2 v}s + e_2 \\ e^{-j\omega r_3 v}s + e_3 \\ e^{-j\omega r_4 v}s + e_4 \\ e_5 \\ e_6 \\ e_7 \\ e_8 \end{bmatrix}, \quad (14)$$

where $s = [s(1), s(2), ..., s(N)] \in \mathbb{C}^{1 \times N}$ is the signal vector and $E = [e_1, e_2, ..., e_8]^T \in \mathbb{C}^{8 \times N}$ is the noise matrix.

According to Eq. (11), for a certain direction vector (θ, ϕ), each element in $A(\theta, \phi)$ are only related to the coordinates of the corresponding array elements. Therefore, based on the positional relationship between the different elements, it is possible to reconstruct the signal of receiving restricted elements from the signal of receiving normal elements.

Suppose that $E = 0$, then, the signal matrix of receiving restricted elements is $X' = [e_5, e_6, e_7, e_8]^T = 0 \in \mathbb{C}^{4 \times N}$ and the coordinates matrix of the corresponding array elements is $BS' = \begin{bmatrix} x_5 & y_5 & z_5 \\ x_6 & y_6 & z_6 \\ x_7 & y_7 & z_7 \\ x_8 & y_8 & z_8 \end{bmatrix}$. Meanwhile, the signal matrix of receiving normal elements $X'' \in \mathbb{C}^{4 \times N}$ can be rewritten as

$$X'' = \begin{bmatrix} e^{-j\omega r_1 v}s + e_1 \\ e^{-j\omega r_2 v}s + e_2 \\ e^{-j\omega r_3 v}s + e_3 \\ e^{-j\omega r_4 v}s + e_4 \end{bmatrix} = \begin{bmatrix} e^{-j\omega[x_1,y_1,z_1]v} \\ e^{-j\omega[x_2,y_2,z_2]v} \\ e^{-j\omega[x_3,y_3,z_3]v} \\ e^{-j\omega[x_4,y_4,z_4]v} \end{bmatrix} s = e^{-j\omega BS''v}s, \quad (15)$$

and the coordinates matrix is $BS'' = \begin{bmatrix} x_1 & y_1 & z_1 \\ x_2 & y_2 & z_2 \\ x_3 & y_3 & z_3 \\ x_4 & y_4 & z_4 \end{bmatrix}$. Divide both sides of Eq. (15) by s, Eq. (15) can be rewritten as

$$\frac{X''}{s} = e^{-j\omega BS''v} \quad (16)$$

where $\frac{X''}{s} = \left[\frac{x''_1}{s}, \frac{x''_2}{s}, \frac{x''_3}{s}, \frac{x''_4}{s}\right]^T$. Further, take the logarithm of both sides of Eq. (16), Eq. (17) is obtained.

$$\log\left(\frac{X''}{s}\right) = -j\omega BS''v. \quad (17)$$

According to Eq. (17), it is easy to find that $-j\omega\boldsymbol{v}$ would be unique and determined if there are 3 non-linearly related vectors in BS''. And then, the reconstructed signal matrix $\hat{\boldsymbol{X}}'$ for receiving restricted elements can be obtained according to $-j\omega\boldsymbol{v}$ and BS'.

As shown in Fig. 2, when the number of elements $M \geq 6$, there are at least 3-row vectors in BS''. Appendix proves that BS'' is a column full rank matrix. Therefore, converting BS''^T into a row simplest form matrix, it can be obtained that

$$[\mathbf{E}, jb] = \mathrm{rref}\left(BS''^T\right), \tag{18}$$

where $\mathrm{rref}(.)$ denotes the primary transformation. $\mathbf{E}$ is the row simplest form matrix of BS''^T. jb is a vector of length 3, and the elements in jb are the columns of the basis vector in $\mathbf{E}$. Then, 3 non-linearly related vectors BS''' in BS'' can be formed by choosing the row vectors corresponding to the elements of jb in BS'', and the signal matrix $\boldsymbol{X}'''$ is also can be formed by choosing the row vectors corresponding to the elements of jb in $\boldsymbol{X}''$. Therefore, $-j\omega\boldsymbol{v}$ can be expressed as

$$-j\omega\boldsymbol{v} = (BS''')^{-1}\log\left(\frac{\boldsymbol{X}'''}{\boldsymbol{s}}\right). \tag{19}$$

Then, combining $-j\omega\boldsymbol{v}$ and BS', the reconstructed signal matrix $\hat{\boldsymbol{X}}'$ of receiving restricted elements can be obtained

$$\hat{\boldsymbol{X}}' = e^{-j\omega BS'\boldsymbol{v}}\boldsymbol{s} = e^{BS'\left(BS'''\right)^{-1}\log\left(\frac{\boldsymbol{x}'''}{\boldsymbol{s}}\right)}\boldsymbol{s}. \tag{20}$$

However, in practice, $\mathbf{E} \neq 0$. Therefore, $\boldsymbol{X}'' = \begin{bmatrix} e^{-j\omega\mathbf{r}_1\boldsymbol{v}}\boldsymbol{s} + \boldsymbol{e}_1 \\ e^{-j\omega\mathbf{r}_2\boldsymbol{v}}\boldsymbol{s} + \boldsymbol{e}_2 \\ e^{-j\omega\mathbf{r}_3\boldsymbol{v}}\boldsymbol{s} + \boldsymbol{e}_3 \\ e^{-j\omega\mathbf{r}_4\boldsymbol{v}}\boldsymbol{s} + \boldsymbol{e}_4 \end{bmatrix}$, and the array output matrix $\hat{\boldsymbol{X}}$ after signal reconstruction can eventually be written as

$$\hat{\boldsymbol{X}} = \begin{bmatrix} \boldsymbol{X}'' \\ \hat{\boldsymbol{X}}' \end{bmatrix}. \tag{21}$$

C. DOA estimation

Comparing Eq. (21) and Eq. (14), the array output has been expanded after signal reconstruction, while the shadow effect is eliminated and the DOF is increased. Substitute Eq. (21) into Eq. (8), the covariance matrix $\hat{R}'_x$ can be rewritten as

$$\hat{R}'_x = \frac{1}{N}\hat{\boldsymbol{X}}\hat{\boldsymbol{X}}^H. \tag{22}$$

And then, the SR-MUSIC-RS method is formed in this paper by searching the peak of the following formula in the range of (Θ, Φ).

$$P_{\mathrm{SR-MUSIC-RS}} = \frac{1}{\boldsymbol{\alpha}^H(\theta, \phi)\hat{U}'_e\hat{U}'^H_e\boldsymbol{\alpha}(\theta, \phi)}, \theta \in \Theta, \phi \in \Phi, \tag{23}$$

where $\hat{U}'_e$ is the noise subspace eigenmatrix of $\hat{R}'_x$, and (θ, ϕ) corresponded to the peak value of $P_{\mathrm{SR-MUSIC-RS}}$ is the estimated DOA. The proposed SR-MUSIC-RS algorithm is described in Algorithm 1.

Algorithm 1 SR-MUSIC-RS algorithm.

Input: The array output matrix $\boldsymbol{X} = [\boldsymbol{x}_1, \boldsymbol{x}_2, ..., \boldsymbol{x}_M]^T$, the position matrix of each element BS and the source signal vector $\boldsymbol{s}$.

1: **Initialization** : The receiving restricted element set $\Xi \in \varnothing$, the receiving normal element $\Psi \in \varnothing$, the approximate range of DOA $(\Theta, \Phi) \in \varnothing$, the frequency-domain matrix $\boldsymbol{Y} = [\boldsymbol{y}_1, \boldsymbol{y}_2, ..., \boldsymbol{y}_M]^T$ using FFT.

2: Calculate the frequency domain energy of each array element: $F_e(m) = \max(|\boldsymbol{y}_m|)$.

3: Update the receiving restricted element set $\Xi = \{BS\}_{LA(m)=0}$ and receiving normal element $\Psi = \{BS\}_{LA(m)=1}$ according to Eq. (13), and the approximate range of DOA (Θ, Φ) according to Eq. (9).

4: Extract the signal matrix of receiving normal elements $\boldsymbol{X}'' = \{\boldsymbol{X}\}_\Psi$ and the corresponding coordinate matrix $BS'' = \{BS\}_\Psi$, and the coordinate matrix of receiving restricted elements $BS' = \{BS\}_\Xi$.

5: Set $[\mathbf{E}, jb] = \mathrm{rref}\left(BS''^T\right)$, $BS''' = \{BS''\}_{jb}$, and $\boldsymbol{X}''' = \{\boldsymbol{X}''\}_{jb}$.

6: Construct the signal matrix $\hat{\boldsymbol{X}}'$ of the receiving restricted elements using Eq. (20) and the array output matrix $\hat{\boldsymbol{X}}$ using Eq. (21).

7: Use MUSIC algorithm to search the peak value of Eq. (23) in the range of (Θ, Φ), and get the corresponding (θ, ϕ) to the peak value.

8: End.

Output: Estimated DOAs: (θ, ϕ).

IV. CRAMER-RAO LOWER BOUND

Due to the impact of noise on received signal of each element, DOA estimation performance of unbiased estimator generally exhibits fluctuations. The CRLB obtained from the inverse of the Fisher information matrix (FIM) can determine a lower bound on the variance of the unbiased algorithms, which can be regarded as the best available accuracy achieved by the best estimator. That is, no unbiased estimator can outperform the CRLB. Therefore, in this paper, the CRLB is used to depict the effect of the restricted signal model used for DOA estimation.

In this paper, the estimated parameters are azimuth and elevation angles (θ, ϕ), the restricted signal model are shown as Eq. (11). Then, the PDF of N samples and (θ, ϕ) in the above received restricted signal model is written as Eq. (24). And the log likelihood function $\ln(p(\boldsymbol{X}; (\theta, \phi)))$ is constructed as

$$\ln(p(\boldsymbol{X}; (\theta, \phi))) = \ln c -$$
$$\frac{1}{2\delta_e^2}\sum_{n=1}^{N}(\boldsymbol{x}(n) - \boldsymbol{A}(\theta, \phi)s(n))^H(\boldsymbol{x}(n) - \boldsymbol{A}(\theta, \phi)s(n)), \tag{25}$$

where $\ln c = \ln\left(\frac{1}{(2\pi\sigma_e^2)^{2/N}}\right)$.

$$p\left(\boldsymbol{X};(\theta,\phi)\right) = \prod_{n=1}^{N} \frac{1}{\sqrt{2\pi\delta_e^2}} \exp\left(-\frac{1}{2\delta_e^2}(\boldsymbol{X}-\boldsymbol{A}s)^H(\boldsymbol{X}-\boldsymbol{A}s)\right)$$
$$= \frac{1}{(2\pi\delta_e^2)^{2/N}} \exp\left(-\frac{1}{2\delta_e^2}\sum_{n=1}^{N}\left(\boldsymbol{x}\left(n\right)-\boldsymbol{A}(\theta,\phi)s\left(n\right)\right)^H\left(\boldsymbol{x}\left(n\right)-\boldsymbol{A}(\theta,\phi)s\left(n\right)\right)\right). \quad (24)$$

Based on Eq. (25), the FIM for $\ln\left(p\left(\boldsymbol{X};(\theta,\phi)\right)\right)$ can be expressed as

$$\text{FIM}_{\text{RS}} = \begin{bmatrix} F_{\theta\theta} & F_{\theta\phi} \\ F_{\phi\theta} & F_{\phi\phi} \end{bmatrix} \in \mathbb{C}^{2\times 2}, \quad (26)$$

where the CRLBs for θ and ϕ are given by $\left[\text{FIM}_{\text{RS}}^{-1}\right]_{11}$ and $\left[\text{FIM}_{\text{RS}}^{-1}\right]_{22}$, respectively. Correspondingly, the CRLB for (θ,ϕ) is given as

$$\text{CRLB}_{\text{RS}} = \left[\text{FIM}_{\text{RS}}^{-1}\right]_{11} + \left[\text{FIM}_{\text{RS}}^{-1}\right]_{22} = \text{tr}\{\text{FIM}_{\text{RS}}^{-1}\}. \quad (27)$$

Further, FIM_{RS} can be calculated as

$$\text{FIM}_{\text{RS}} = -\begin{bmatrix} E\left[\frac{\partial^2 \ln(p(\boldsymbol{X};(\theta,\phi)))}{\partial\theta^2}\right] & E\left[\frac{\partial^2 \ln(p(\boldsymbol{X};(\theta,\phi)))}{\partial\theta\partial\phi}\right] \\ E\left[\frac{\partial^2 \ln(p(\boldsymbol{X};(\theta,\phi)))}{\partial\phi\partial\theta}\right] & E\left[\frac{\partial^2 \ln(p(\boldsymbol{X};(\theta,\phi)))}{\partial\phi^2}\right] \end{bmatrix}. \quad (28)$$

Substitute Eq. (25) into Eq. (28), the second derivative of $\ln\left(p\left(\boldsymbol{X};(\theta,\phi)\right)\right)$ with respect to θ can be written as Eq. (29)

Due to the zero mean Gaussian noise, the sum of the N samples received signal can be written as

$$\sum_{n=1}^{N}\boldsymbol{x}(n) = \sum_{n=1}^{N}\boldsymbol{A}(\theta,\phi)s\left(n\right) + \sum_{n=1}^{N}\boldsymbol{e}(n)$$
$$\approx \sum_{n=1}^{N}\boldsymbol{A}(\theta,\phi)s\left(n\right) = \boldsymbol{A}(\theta,\phi)\sum_{n=1}^{N}s\left(n\right). \quad (30)$$

Meanwhile, the sum of square of the N samples source signal can be written as

$$\sum_{n=1}^{N}s^2(n) = N\,\text{var}\left(s(n)\right) = N\delta_s^2. \quad (31)$$

Therefore, substituted Eq. (30) and Eq. (31) into Eq. (29), $F_{\theta\theta}$ can be expressed as

$$F_{\theta\theta} = -E\left[\frac{\partial^2 \ln\left(p\left(\boldsymbol{X};(\theta,\phi)\right)\right)}{\partial\theta^2}\right]$$
$$= \frac{N\delta_s^2}{2\delta_e^2}\left(2\frac{\partial\boldsymbol{A}^H}{\partial\theta}\frac{\partial\boldsymbol{A}}{\partial\theta}\right) \quad (32)$$
$$= \frac{N\delta_s^2}{\delta_e^2}\left\|\frac{\partial\boldsymbol{A}}{\partial\theta}\right\|^2,$$

where $\|.\|$ denotes the second norm.

Similarly, the rest entries of FIM_{RS} can be calculated as follows:

$$F_{\theta\phi} = \frac{N\delta_s^2}{2\delta_e^2}\left(\frac{\partial\boldsymbol{A}^H}{\partial\theta}\frac{\partial\boldsymbol{A}}{\partial\phi} + \frac{\partial\boldsymbol{A}^H}{\partial\phi}\frac{\partial\boldsymbol{A}}{\partial\theta}\right), \quad (33)$$

$$F_{\phi\theta} = \frac{N\delta_s^2}{2\delta_e^2}\left(\frac{\partial\boldsymbol{A}^H}{\partial\phi}\frac{\partial\boldsymbol{A}}{\partial\theta} + \frac{\partial\boldsymbol{A}^H}{\partial\theta}\frac{\partial\boldsymbol{A}}{\partial\phi}\right), \quad (34)$$

$$F_{\phi\phi} = \frac{N\delta_s^2}{\delta_e^2}\left\|\frac{\partial\boldsymbol{A}}{\partial\phi}\right\|^2. \quad (35)$$

And then, the CRLB of the restricted signal model is simply obtained according to Eq. (27).

Due to the different array responses, the Fisher matrix of general signal model can be also calculated as

$$\text{FIM}_{\text{GS}} =$$
$$\frac{N\delta_s^2}{\delta_e^2}\begin{bmatrix} \left\|\frac{\partial\boldsymbol{\alpha}}{\partial\theta}\right\|^2 & \frac{1}{2}\left(\frac{\partial\boldsymbol{\alpha}^H}{\partial\theta}\frac{\partial\boldsymbol{\alpha}}{\partial\phi} + \frac{\partial\boldsymbol{\alpha}^H}{\partial\phi}\frac{\partial\boldsymbol{\alpha}}{\partial\theta}\right) \\ \frac{1}{2}\left(\frac{\partial\boldsymbol{\alpha}^H}{\partial\phi}\frac{\partial\boldsymbol{\alpha}}{\partial\theta} + \frac{\partial\boldsymbol{\alpha}^H}{\partial\theta}\frac{\partial\boldsymbol{\alpha}}{\partial\phi}\right) & \left\|\frac{\partial\boldsymbol{\alpha}}{\partial\phi}\right\|^2 \end{bmatrix}. \quad (36)$$

And the CRLB of general signal model is given as

$$\text{CRLB}_{\text{GS}} = \text{tr}\{\text{FIM}_{\text{GS}}^{-1}\}. \quad (37)$$

V. SIMULATIONS

Consider the DOA estimation scenario as illustrated in Fig. 1, the performance of the proposed SR-MUSIC-RS method is verified and evaluated in this section. All simulations are carried out using MATLAB R2016a on the computer with an Intel i7-10700 processor and 16G memory. The root mean squared error (RMSE) is used to assess DOA estimation performance, which is defined as

$$\text{RMSE} = \sqrt{\frac{1}{2}\left(\left(\theta-\widehat{\theta}\right)^2 + \left(\phi-\widehat{\phi}\right)^2\right)}, \quad (38)$$

where (θ,ϕ) is the true DOA of source, and $\left(\widehat{\theta},\widehat{\phi}\right)$ is the estimation of (θ,ϕ).

For comparison under restricted signal model, the behaviors of C-MUSIC-RS, S-MUSIC-RS, GRNN-RS and CRLB_{RS} are presented. Further, under general signal model, C-MUSIC-GS and CRLB_{GS} are also simulated. The radius and height of CCA are $d = 0.1$ m and $h = 0.1$ m. Different DOAs randomly selected in the omnidirectional space are used as DOAs of the target signal, and the simulation results are obtained by averaging results among all the DOAs. Each simulation result is the average of 3000 Monte Carlo experiments. The angle search grid interval is set to $1°$, and the range of azimuth angle and elevation angle are $[0°, 360°)$ and $[0°, 180°)$, respectively. In addition, for GRNN-RS method, the $M \times M$ covariance matrix containing the real and imaginary parts is reshaped as a $2MM \times 1$ input feature to input to GRNN, and the spread is set to 0.1. The total dataset consists of 64800 data samples

$$\frac{\partial^2 \ln\left(p\left(\boldsymbol{X};(\theta,\phi)\right)\right)}{\partial\theta^2} = \frac{\partial}{\partial\theta}\left(\frac{\partial\ln\left(p\left(\boldsymbol{X};(\theta,\phi)\right)\right)}{\partial\theta}\right)$$

$$= \frac{\partial}{\partial\theta}\left(-\frac{1}{2\delta_e^2}\sum_{n=1}^{N}\left(-\boldsymbol{x}^H\frac{\partial\boldsymbol{A}}{\partial\theta}s - \frac{\partial\boldsymbol{A}^H}{\partial\theta}s^H\boldsymbol{x} + \frac{\partial\boldsymbol{A}^H}{\partial\theta}\boldsymbol{A}s^2 + \boldsymbol{A}^H\frac{\partial}{\partial\theta}s^2\right)\right) \tag{29}$$

$$= -\frac{1}{2\delta_e^2}\sum_{n=1}^{N}\left(-\boldsymbol{x}^H\frac{\partial^2\boldsymbol{A}}{\partial\theta^2}s - \frac{\partial^2\boldsymbol{A}^H}{\partial\theta^2}s^H\boldsymbol{x} + \frac{\partial^2\boldsymbol{A}^H}{\partial\theta^2}\boldsymbol{A}s^2 + 2\frac{\partial\boldsymbol{A}^H}{\partial\theta}\frac{\partial\boldsymbol{A}}{\partial\theta}s^2 + \boldsymbol{A}^H\frac{\partial^2\boldsymbol{A}}{\partial\theta^2}s^2\right).$$
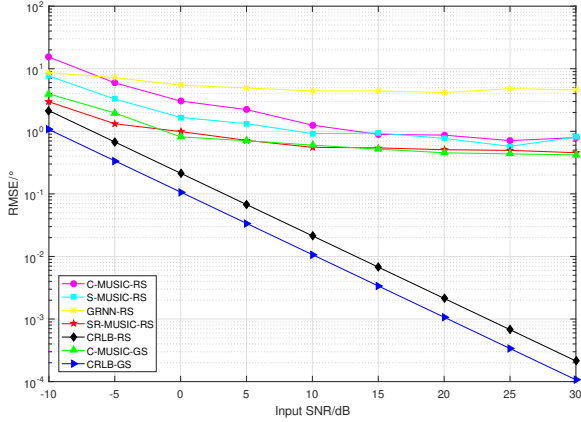
Fig. 5. Comparison of RMSEs of different DOA estimation methods as a function of different input SNRs, $M = 8$, $N = 1000$.
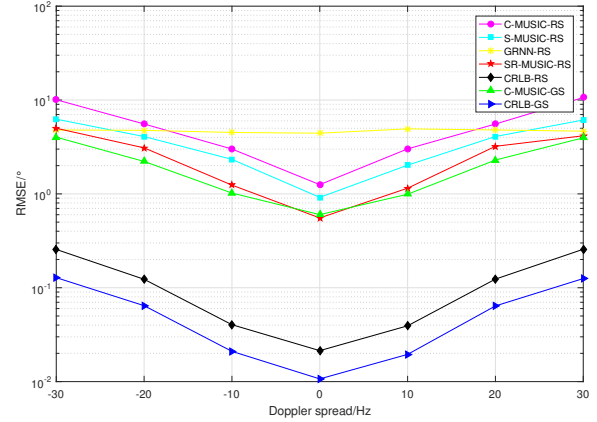
Fig. 6. Comparison of RMSEs of different DOA estimation methods as a function of different Doppler spread, SNR = 10 dB, $N = 1000$, $M = 8$.

and is divided into training, validation, and test sets by a ratio of 7:2:1. One signal source is considered in the simulation, and the sound velocity is set to 340 m/s. If not specified, the Doppler spread is set to 0 Hz.

In the following two subsections, the simulations are performed with artificial target signal and experimentally collected target signal respectively.

A. Simulations with artificial target signal

In this subsection, continuous Sinusoidal signal is adopted as artificial target signal to generate CCA received signals, which is mixed by additive white Gaussian noise (AWGN) for performance evaluation of the proposed method under different signal-to-noise ratio (SNR). The frequency of continuous Sinusoidal signal is 1500 Hz and the sampling frequency is 96 kHz.

Fig. 5 shows the output RMSEs versus the SNR for different DOA estimation methods with the number of array elements $M = 8$ and the length of samples $N = 1000$. The input SNR is defined as SNR $= 10\log_{10}\left(\delta_s^2/\delta_e^2\right)$, ranging from -10 dB to 30 dB with a step size of 5 dB. It can be seen from the figure that the RMSEs of most algorithms gradually decrease with the increase in the input SNR, while the RMSE of GRNN-RS decrease slightly. The reason is that the GRNN-RS method is sensitive to different environments and is difficult to learn the mapping relationship under different input SNR. Also, the RMSEs of the proposed SR-MUSIC-RS are lower than that of C-MUSIC-RS, S-MUSIC-RS, and GRNN-RS algorithms.

This is because that SR-MUSIC-RS reconstructs the received signal of receiving restricted elements, thereby eliminating the "shadow effect". However, C-MUSIC-RS and GRNN-RS estimate the DOA directly from the array output, the accuracy of the DOA estimation would inevitably be severely affected by the noise of receiving restricted elements. And, S-MUSIC-RS estimates the DOA only from the signals of receiving normal elements, resulting in losing half of the array gain. Furthermore, as shown in Fig. 5, the RMSEs of SR-MUSIC-RS are lower than C-MUSIC-GS when SNR $<$ 0 dB. And when SNR $\geq$ 0 dB, SR-MUSIC-RS and C-MUSIC-GS obtain a similar DOA estimation accuracy. The results prove the robustness of the proposed SR-MUSIC-RS for CCA with receiving restricted elements, and shows that the proposed algorithm can achieve a satisfactory DOA estimation performance.

Although the impact of "Doppler effect" can be addressed by doppler estimation and compensation algorithms, Fig. 6 still shows the comparison of RMSEs versus different Doppler spread for different DOA estimation methods. The input SNR is 10 dB with the number of array elements $M = 8$ and the length of samples $N = 1000$. The Doppler spread is imposed on the received signal by artificial resampling and set to range from -30 Hz to 30 Hz with a step size of 10 Hz. Note that the dataset of GRNN-RS is updated to contain all the artificial Doppler spreads with the same total sample number of 64800 to keep the same model complexity, corresponding to much fewer data samples at each Doppler level.
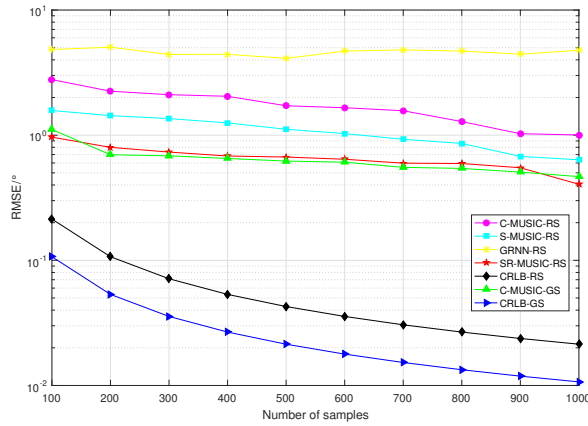
Fig. 7. Comparison of RMSEs of different methods as a function of different numbers of samples, $M = 8$, SNR = 10 dB.

Fig. 8. Comparison of RMSEs of different DOA estimation methods as a function of different numbers of array elements, SNR = 10 dB, $N = 1000$.

It can be seen that the RMSEs of most algorithms seriously decline with an increase in Doppler spread. This is because the DOAs are estimated directly from the received signal without Doppler compensation, which inevitably reduces the DOA estimation accuracy. However, SR-MUSIC-RS and C-MUSIC-GS obtain a similar DOA estimation accuracy and are smaller than other methods, which further proves the effectiveness of the proposed algorithm. Meanwhile, one may observe that the RMSEs of GRNN-RS are relatively high and almost unchanged along different Doppler, the reason is that the number of data samples at each Doppler level is highly limited thus cannot guarantee training quality of the model. The rapidly increasing dimension of data samples caused by Doppler poses a significant challenge to the learning-based DOA algorithm.

Fig. 7 provides the output RMSEs versus the different number of samples N for different DOA estimation methods with the number of array elements $M = 8$ and the input SNR = 10 dB. The number of samples is ranging from 100 to 1000 with a step size of 100. It can be seen from the figure that the RMSEs of most algorithms gradually decrease with the increase in the number of samples, while the RMSE of GRNN-RS is almost unchanged. It means that the number of samples has little effect on the accuracy of GRNN-RS method. And the RMSEs of SR-MUSIC-RS and C-MUSIC-GS are always lower for each number of samples than that of C-MUSIC-RS, S-MUSIC-RS and GRNN-RS. The reason for this is that the signal reconstruction of the proposed algorithm compensates for the receiving restricted elements. Thus, the proposed algorithm can achieve approximate DOA estimation performance of C-MUSIC-GS and is not sensitive to the length of samples. In addition, the RMSEs of SR-MUSIC-RS are slightly higher than that of C-MUSIC-GS. Considering the effect of noise on the signal reconstruction of the proposed algorithm, the higher RMSEs of the proposed algorithm are acceptable.

Shown in Fig. 8 is the output RMSEs versus the different number of array elements M for different DOA estimation methods with the input SNR = 10 dB and the length of
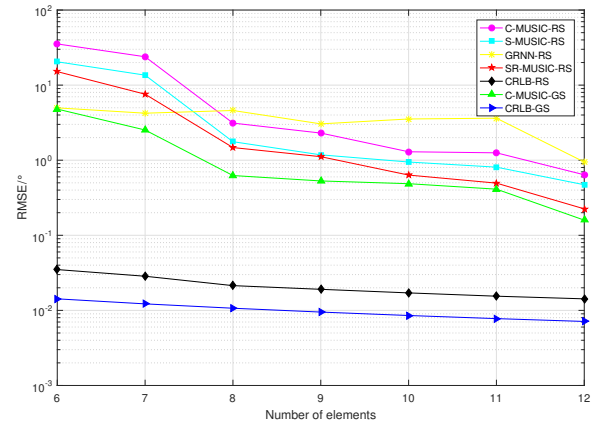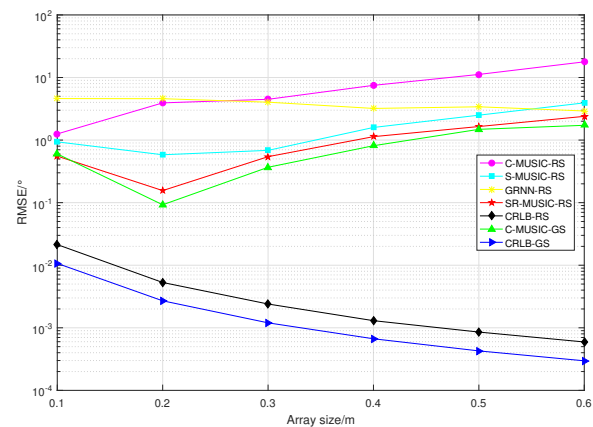
Fig. 9. Comparison of RMSEs of different DOA estimation methods as a function of different array sizes, SNR = 10 dB, $N = 1000$, $M = 8$.

samples $N = 1000$. The number of array elements is ranging from 6 to 12 with a step size of 1. It can be seen from the figure that the RMSEs of all algorithms decrease with the increase in the number of array elements, and the performance of SR-MUSIC-RS and C-MUSIC-GS are much better than that of C-MUSIC-RS, S-MUSIC-RS, and GRNN-RS. Although the RMSEs of SR-MUSIC-RS and GRNN-RS are similar when $M = 6$ and are smaller than that of C-MUSIC-RS and S-MUSIC-RS, the performance of SR-MUSIC-RS can obtain a lower RMSE at a relatively small number of elements, i.e. $M = 10$ for SR-MUSIC-RS versus $M = 12$ for C-MUSIC-RS, S-MUSIC-RS, and GRNN-RS. The results verify the effectiveness of the proposed algorithm and prove that the proposed algorithm does improve the DOF of the array.

On the other hand, it can be seen from Fig. 8 that the DOA estimation performance of DOA estimation methods increases with the increase in number of array elements, nonetheless, it will inevitably increase the computational complexity. Therefore, in the actual engineering, the estimation accuracy and computational complexity should be comprehensively considered to select the appropriate number of array elements.

(a) Time-domain waveform

(b) Time-frequency spectrum
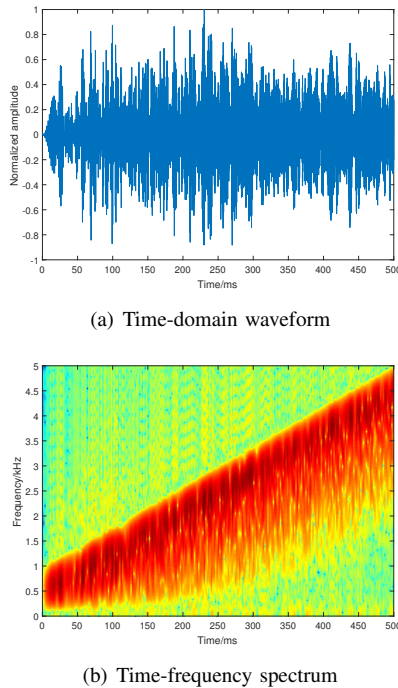
Fig. 10. Experimentally collected LFM signal in reverberation laboratory.

(a) Time-domain waveform

(b) Time-frequency spectrum
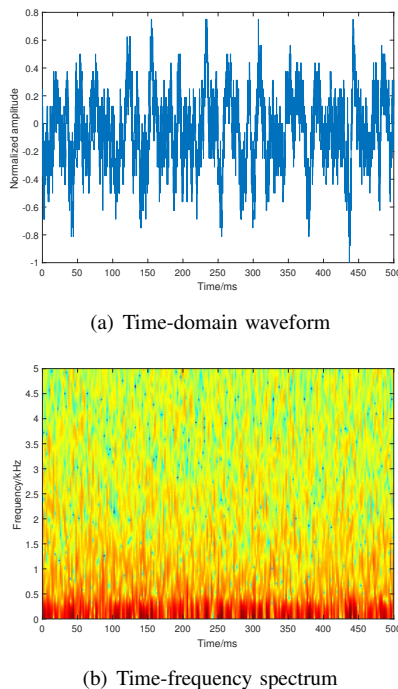
Fig. 11. Experimentally collected environmental noise in reverberation laboratory.

It is widely known that array size is one of the key factors affecting DOA estimation performance. When the spatial sampling theorem is satisfied, that is $d' \leq \frac{\lambda}{2}$ where d' is element spacing, the performance of the DOA estimation algorithm would increase with the increase in the array size. To verify the DOA estimation performance under different sizes of CCA, Fig. 9 shows the comparison of RMSEs as a function of
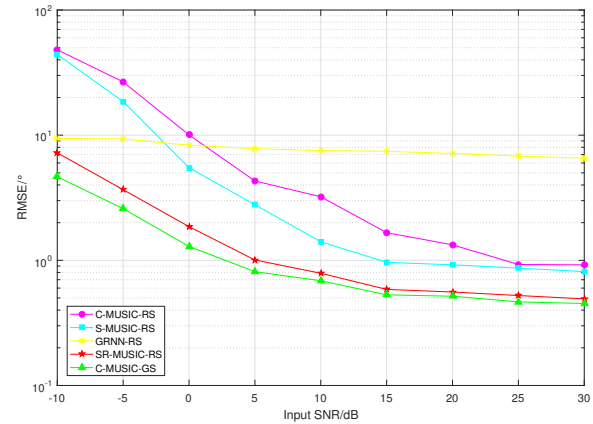
Fig. 12. Comparison of RMSEs of different DOA estimation methods as a function of different input SNRs.

different array sizes. The X-axis represents the size of d and h, i.e. $d = h = 0.1$ m, $d = h = 0.2$ m, ..., $d = h = 0.6$ m. The input SNR is 10 dB with the number of array elements $M = 8$ and the length of samples $N = 1000$. It can be seen that the performance of SR-MUSIC-RS and C-MUSIC-GS algorithms varies with array size, while the others are almost unchanged. The curves of SR-MUSIC-RS and C-MUSIC-G also show that there is an appropriate array size between $d = h = 0.1$ m and $d = h = 0.3$ m can further optimize the DOA estimation performance. According to the source signal parameters set in simulations, the range of the optimal array size is exactly half of the signal wavelength, which conforms to the spatial sampling theorem. Therefore, we should choose the size of array as close as possible to half of the signal wavelength. However, the large sizes are not conducive to the miniaturization of the array. Thus, the size of array should be selected according to the requirements for miniaturization and precision.

In addition, it is also observed from the above simulations that, the RMSEs of most algorithms finally converge between 10^0 and 10^{-1}, this is because that we set the angle search grid interval to $1°$, resulting in a lower accuracy. It is not difficult to prove that reducing the angle search grid interval will greatly improve the DOA estimation accuracy, but this will inevitably increase the computational complexity. Considering the need for UAVs sound source localization accuracy in practical engineering, the above DOA estimation accuracy is sufficient. Moreover, the accuracy of GRNN-RS is poor and changes little with different external factors, such as input SNR, number of samples or elements, etc. Due to the various factors affecting the performance of DOA estimation, it is difficult to obtain comprehensive enough data for GRNN-RS training. Thus, the RMSEs of GRNN-RS are almost higher than other algorithms and hardly change with external factors.

B. Simulations with experimentally collected target signal

In this subsection, linear frequency modulation (LFM) signal experimentally collected in a reverberation laboratory with a reverberation time of 0.4 s is adopted as target signal to

generate CCA received signals for performance evaluation. The frequency range and time duration of the LFM signal are 500 Hz $\sim$ 4.5 kHz and 0.5 s respectively, which is collected at a distance of $R = 5$ m with a sampling frequency of 16 kHz.

As the radius and height of CCA are $d = 0.1$ m and $h = 0.1$ m respectively, both of which are much shorter than the distance $R = 5$ m away from the source, the reverberation pattern of each array element is assumed to be the same, corresponding to a reverberation of 0.4 s. We also collected a practical environmental noise in the same reverberation laboratory as the additive noise to generate noisy signal of different SNR. Shown in Fig. 10 and Fig. 11 are the time-domain waveform and time-frequency spectrum of the experimentally collected LFM signal and practical environmental noise, respectively. It can be seen that experimentally collected target signal is deteriorated by both reverberation and noise.

Fig. 12 shows the comparison of output RMSEs of the five algorithms with different input SNR, where the received LFM signal shown in Fig. 10 is used as the target signal and the received practical environmental noise shown in Fig. 11 is used as the additive noise. The input SNR is defined in **Section V. A**, the number of array elements is $M = 8$, and the length of samples is $N = 1000$. The other parameter settings are the same as those in **Section V. A**. It can be seen from Fig. 12 that the results are similar to those of Fig. 5, that is, the proposed SR-MUSIC-RS under restricted signal model also can achieve a similar DOA estimation performance compared with the C-MUSIC-GS under general signal model. The result evidences the superiority of the proposed algorithm.

C. Complexities

Table I lists the complexities and average running times of MUSIC-based algorithms, i.e. C-MUSIC-RS, C-MUSIC-GS, S-MUSIC-RS, and SR-MUSIC-RS, where M is the number of elements, P and Q are the search number of azimuth and elevation angle, respectively. Since all the algorithms mentioned in this paper are mainly concentrated in the search process, the computational complexity in the search process is only considered here. According to the parameter settings, C-MUSIC-RS and C-MUSIC-GS have a same computational complexity since the calculation process is the same. And their computational complexities are $O(P * Q * M^2(M-1))$ which are mainly in the multiplication of noise subspace matrix. Since S-MUSIC-RS only calculates the signals of the received normal elements, the computational complexity is $O(P * Q * (M/2)^2(M/2-1))$. The proposed SR-MUSIC-RS algorithm reduces the search range by the detection of receiving restricted elements, thus, the computational complexity is $O((P/M) * Q * M^2(M-1))$.

In terms of computational complexity, it can be seen from Table I that the average running time of SR-MUSIC-RS is an order smaller than that of other algorithms, indicating much less computational overhead in practical implementation.

VI. CONCLUSION

In view of the booming development of UAVs in various fields, sound source localization with CCA onboard UAVs is

TABLE I
COMPLEXITIES AND AVERAGE RUNNING TIMES OF DIFFERENT DOA ESTIMATION METHODS

Algorithm	Complexity	Ave-time (s)
C-MUSIC-RS	$O(P * Q * M^2(M-1))$	0.4006
C-MUSIC-GS	$O(P * Q * M^2(M-1))$	0.39959
S-MUSIC-RS	$O(P * Q * (M/2)^2(M/2-1))$	0.36188
SR- MUSIC-RS	$O((P/M) * Q * M^2(M-1))$	0.05411

receiving more and more interests from research community and industry. However, shadow effects associated with CCA impose significant constraint upon the performance of sound source localization.

In this paper, CCA sound source localization in the presence of shadow elements is investigated by proposing a signal reconstruction-based DOA estimation method. Different from the conventional approaches that directly ignore shadowed elements, the signals of receiving restricted elements are reconstructed based on the signals of receiving normal elements to eliminate the shadow effect.

The 2-D CRLB analysis and simulations show that, compared with the existing algorithms, the proposed SR-MUSIC-SR algorithm is capable of achieving satisfactory sound localization performance with lower complexity at the presence of shadow elements.

APPENDICES

This appendix proves that BS'' is a column full rank matrix

Take an 8 elements array as an example, the polar coordinates of BS'' can be written as

$$BS'' = \begin{bmatrix} x_1 & y_1 & z_1 \\ x_2 & y_2 & z_2 \\ x_3 & y_3 & z_3 \\ x_4 & y_4 & z_4 \end{bmatrix} = \begin{bmatrix} 0 & \frac{\pi}{2} & \sqrt{d^2+h^2} \\ \frac{\pi}{4} & \tan^{-1}\left(\frac{d}{h}\right) & \sqrt{d^2+h^2} \\ \frac{\pi}{2} & \frac{\pi}{2} & \sqrt{d^2+h^2} \\ \frac{3\pi}{4} & \tan^{-1}\left(\frac{d}{h}\right) & \sqrt{d^2+h^2} \end{bmatrix}. \tag{39}$$

Set $\theta_1 = 0$, $\theta_2 = \frac{\pi}{4}$, $\theta_3 = \frac{\pi}{2}$, $\theta_4 = \frac{3\pi}{4}$, $\phi_1 = \frac{\pi}{2}$, $\phi_2 = \tan^{-1}\left(\frac{d}{h}\right)$, $r = \sqrt{d^2+h^2}$, then the elementary transformation of BS''^T can be expressed as

$$BS''^T = \begin{bmatrix} \theta_1 & \theta_2 & \theta_3 & \theta_4 \\ \phi_1 & \phi_2 & \phi_1 & \phi_2 \\ r & r & r & r \end{bmatrix} \overset{r_1 \rightleftharpoons r_3}{\sim} \begin{bmatrix} r & r & r & r \\ \phi_1 & \phi_2 & \phi_1 & \phi_2 \\ 0 & \theta_2 & \theta_3 & \theta_4 \end{bmatrix}$$

$$\overset{r_2 - \frac{\phi_1}{r} r_1}{\sim} \begin{bmatrix} r & r & r & r \\ 0 & \phi_2 - \phi_1 & 0 & \phi_2 - \phi_1 \\ 0 & \theta_2 & \theta_3 & \theta_4 \end{bmatrix}$$

$$\overset{r_3 - \frac{\theta_2}{\phi_2 - \phi_1} r_2}{\sim} \begin{bmatrix} r & r & r & r \\ 0 & \phi_2 - \phi_1 & 0 & \phi_2 - \phi_1 \\ 0 & 0 & \theta_3 & \theta_4 - \theta_2 \end{bmatrix}. \tag{40}$$

According to Fig. 3, it is obvious that r, $\phi_2 - \phi_1$ and θ_3 are all no-zero elements, that is rank $\left(BS''^T\right) = 3$. Therefore, BS''^T is the row full rank matrix, and BS'' is the column full rank matrix. Similarly, it can be proved that when $M \geq 6$, BS'' is a column full rank matrix.

REFERENCES

[1] J. Cong, X. Wang, C. Yan, L. T. Yang, M. Dong and K. Ota, "CRB Weighted Source Localization Method Based on Deep Neural Networks in Multi-UAV Network," *IEEE Internet of Things Journal*, doi: 10.1109/JIOT.2022.3150794.

[2] R. Akter, M. Golam, V. S. Doan, J. M. Lee and D. S. Kim, "IoMT-Net: Blockchain Integrated Unauthorized UAV Localization Using Lightweight Convolution Neural Network for Internet of Military Things," *IEEE Internet of Things Journal*, doi: 10.1109/JIOT.2022.3176310.

[3] A. Albanese, V. Sciancalepore and Xavier Costa-Pérez, "SARDO: An Automated Search-and-Rescue Drone-Based Solution for Victims Localization," *IEEE Transactions on Mobile Computing*, vol. 21, no. 9, pp. 3312-3325, Sep. 2022.

[4] W. Manamperi, T. D. Abhayapala, J. Zhang and P. N. Samarasinghe, "Drone Audition: Sound Source Localization Using On-Board Microphones," *IEEE-ACM Transactions on Audio Speech and Language Processing*, vol. 30, pp. 508-519, Jan. 2022.

[5] S. V. Sibanyoni, D. T. Ramotsoela, B. J. Silva and G. P. Hancke, "A 2-D Acoustic Source Localization System for Drones in Search and Rescue Missions," *IEEE Sensors Journal*, vol. 19, no. 1, pp. 332-341, Jan. 2019.

[6] R. Schmidt, "Multiple emitter location and signal parameter estimation," *IEEE Transactions on Antennas & Propagation*, vol. 34, no. 3, pp. 276-280, Mar. 1986.

[7] W. Zhu, M. Zhang, C. Wu, and L. Zeng, "Broadband direction of arrival estimation based on convolutional neural network," *IEICE Transactions on Communications*, vol. E103.B, no. 3, pp. 148-154, 2020.

[8] Y. Wang and H. Peng, "Underwater acoustic source localization using generalized regression neural network, *The Journal of the Acoustical Society of America*, vol. 143, no. 4, pp. 2321-2331, 2018.

[9] Z. Q. Wang, X. Zhang, and D. Wang, "Robust speaker localization guided by deep learning-based time-frequency masking, *IEEE/ACM Transactions on Audio, Speech, and Language Processing,* vol. 27, no. 1, pp. 178-188, 2019.

[10] M. Comisso and R. Vescovo, "Fast co-polar and cross-polar 3D pattern synthesis with dynamic range ratio reduction for conformal antenna arrays," *IEEE Trans. Antennas and Propagation*, vol. 61, no. 2, pp. 614-626, Oct. 2013.

[11] Q. Q. He, B. Z. Wang and W. Shao, "Radiation pattern calculation for arbitrary conformal arrays that include mutual-coupling effects," *IEEE Antennas Propag. Mag.*, vol. 52, no. 2, pp. 57-63, Apr. 2010.

[12] X. Lan, L. Wang, Y. Wang, C. Choi and D. Choi, "Tensor 2-D DOA Estimation for a Cylindrical Conformal Antenna Array in a Massive MIMO System Under Unknown Mutual Coupling," *IEEE Access*, vol. 6, pp. 7864-7871, Jan. 2018.

[13] X. W. Zhang, G. S. Liao, Z. W. Yang and S. W. Li, "Parameter estimation based on Hough transform for airborne radar with conformal array," *Digital Signal Processing*, vol. 66, no. 1, pp. 1-10, Dec. 2020.

[14] D. Sun, C. Ma and J. Mei, "The deconvolved conventional beamforming for conformal array," *The Journal of the Acoustical Society of America*, vol. 146, no. 4, pp. 3090-3090, Oct. 2019.

[15] M. Sharifi and P. Rezaei, "Conformal antenna array radiation pattern synthesis by tilt correction to improve Direction-of-Arrival estimation accuracy," *Electromagnetics*, vol. 40, no. 1, pp. 1-14, Apr. 2020.

[16] S. Mohammadi, A. Ghani and S. H. Sedighy, "Direction-of-Arrival Estimation in Conformal Microstrip Patch Array Antenna," *IEEE Transactions on Antennas and Propagation*, vol. 66, no. 1, pp. 511-515, Jan. 2018.

[17] X. Y. Lan, Y. F. Li and Y. Chen, "A novel 2D DOA estimation via tensor modeling for cylindrical conformal array," in *2017 9th International Conference on Wireless Communications and Signal Processing (WCSP)*, 11-13 Oct. 2017, Nanjing, China

[18] M. J. Wu, X. F. Zhang, J. J. Huang and N. C. Yuan, "DOA estimation of cylindrical conformal array based on geometric algebra," *International Journal of Antennas and Propagation*, vol. 2016, pp. 1-9, Jan. 2016.

[19] M. C. Fu, Z. Zheng and We. Q. Wang, "2-D DOA Estimation for Nested Conformal Arrays via Sparse Reconstruction," *IEEE Communications Letters*, vol. 25, no. 3, pp. 980-984, Mar. 2021.

[20] C. Liu and S. N. Yin, "Direction Finding for Conformal Array in the Presence of Array Perturbations," in *2015 2nd International Conference on Information Science and Control Engineering*, 24-26 Apr. 2015, Shanghai, China.

[21] X. F. Gao, P. Li, X. H. Hao, G. L. Li and Z. J. Kong, "A novel DOA estimation algorithm using directional antennas in cylindrical conformal arrays," *Defence Technology*, vol. 17, no. 3, pp. 1042-1051, Jun. 2021.

[22] P. Yang, F. Yang and Z. P. Nie. "DOA estimation using MUSIC algorithm on a cylindrical conformal array," in *2007 IEEE Antennas and Propagation Society International Symposium*, 09-15 Jun. 2007, Honolulu, HI.

[23] P. Yang, F. Yang and Z. P. Nie, "DOA Estimation with Sub-Array Divided Technique and Interpolated Esprit Algorithm on a Cylindrical Conformal Array Antenna," *Progress in Electromagnetics Research*, vol. 103, pp. 201-216, Jan. 2010.

[24] P. Alinezhad, S. Seydnejad and D. A. Moghadam, "DOA estimation in conformal arrays based on the nested array principles," *Digital Signal Processing*, vol. 2016, no. 50, pp. 191-202, Jan. 2016.

[25] K. Yang, Z. Q. Zhao, W. Yang and Z. P. Nie, "Direction of arrival estimation on cylindrical conformal array using RARE," *Journal of Systems Engineering and Electronics*, vol. 22, no. 5, pp. 767772, Oct. 2011.

Jiaheng Li received the Master's degree in computer science and technology, Qingdao University of Science and Technology, Qingdao, China, in 2020. He is currently working toward the Ph.D. degree with the Xiamen University, Xiamen, China. He is a reviewer of IEEE Transactions on Vehicular Technology. His current research interests include underwater acoustic communications, array signal processing, DOA estimation.

Feng Tong (Member, IEEE) received the Ph.D. degree in underwater acoustics from Xiamen University, Xiamen, China, in 2000. From 2000 to 2002, he was a Postdoctoral Fellow with the Department of Radio Engineering, Southeast University, Nanjing, China. From January 2003 to July 2004, he was a Research Associate with the Department of Manufacturing Engineering and Engineering Management, City University of Hong Kong, Hong Kong. From December 2009 to December 2010, he was a Visiting Scholar with the Department of Computer Science and Engineering, University of California San Diego, La Jolla, CA, USA. He is currently a Professor with the Department of Applied Marine Physics and Engineering, Xiamen University. His research interests include underwater acoustic communication and acoustic signal processing. He is a Council Member of the Acoustical Society of China, and he serves on the Editorial Board for the JOURNAL OF MARINE SCIENCE AND APPLICATION.

Yuehai Zhou (Member, IEEE) received the bachelor's, master's, and Ph.D. degrees in marine sciences from the College of Ocean and Earth Sciences, Xiamen University, Xiamen, China, in 2010, 2013, and 2018, respectively. From February 2016 to January 2018, he was a Visiting Student with the Department of Electrical and Computer Engineering, The University of Alabama, Tuscaloosa, AL, USA. From November 2018 to January 2020, he was a Postdoctoral Researcher with the Acoustic and Navigation Laboratory, University of Haifa, Haifa, Israel. Currently, he is an Associate Professor with College of Ocean and Earth Sciences, Xiamen University. His research interests are underwater acoustic signal processing, underwater acoustic network, and underwater acoustic modem design.

Yi Yang Yi Yang received the Masters degree in Mechanical Design and Theory from Northeastern University, Shenyang, China in 2011. From 2011 to 2012, he worked as a R&D Engineer at Center of Automatic Instruments and Meters, Northeastern University. From 2012, He works at Shenyang Institute of Automation, Chinese Academy of Sciences. He is currently an Associate Professor in Oceanic Underwater Robot Technology and Engineering Department, Shenyang Institute of Automation, Chinese Academy of Sciences. His research interests include mini AUV and AUV swarms, air-water trans-domain unmanned vehicles, underwater sensing and communication technologies.

Zhiqiang Hu received the Ph.D degree in Mechatronic Engineering from Shenyang Institute of Automation, Chinese Academy of Sciences in 2013. He has been working at Shenyang Institute of Automation, Chinese Academy of Sciences since 2002 till now. He is now a Professor as well as the Dean of Oceanic Underwater Robot Technology and Engineering Department, Shenyang Institute of Automation, Chinese Academy of Sciences. His research interests include Unmanned Underwater Vehicles, AUV swarms, air-water trans-domain unmanned vehicles.